Macromolecules

ARTICLE

pubs.acs.org/Macromolecules

Morphology Development in Model Polyethylene via Two-Dimensional Correlation Analysis

Diana S. Smirnova,[†] Julia A. Kornfield,[*,†] and David J. Lohse[‡]

[†]Division of Chemistry and Chemical Engineering, California Institute of Technology, Pasadena, California 91125, United States

[‡]ExxonMobil Research and Engineering, Annandale, New Jersey 08801, United States

ABSTRACT: Two-dimensional (2D) correlation analysis is applied to synchrotron X-ray scattering data to characterize morphological regimes during nonisothermal crystallization of a model ethylene copolymer (hydrogenated polybutadiene, HPBD). The 2D correlation patterns highlight relationships among multiple characteristics of structure evolution, particularly the extent to which separate features change simultaneously versus sequentially. By visualizing these relationships during cooling, evidence is obtained for two separate physical processes occurring in what is known as "irreversible crystallization" in random ethylene copolymers. Initial growth of primarily lamellae into unconstrained melt ("primary-irreversible crystallization") is distinguished from subsequent secondary lamellae formation in the constrained, noncrystalline regions between the primary lamellae ("secondary-irreversible crystallization"). At successively lower temperatures ("reversible crystallization"), growth of the crystalline reflections is found to occur simultaneously with the change in shape of the amorphous halo, which is inconsistent with the formation of an additional phase. Rather, the synchronous character supports the view that growth of frustrated crystals distorts the adjacent noncrystalline material. Furthermore, heterocorrelation analysis of small-angle and wide-angle X-ray scattering data from the reversible crystallization regime reveals that the size of new crystals is consistent with fringed-micellar structures (~9 nm). Thus, 2D correlation analysis provides new insights into morphology development in polymeric systems.

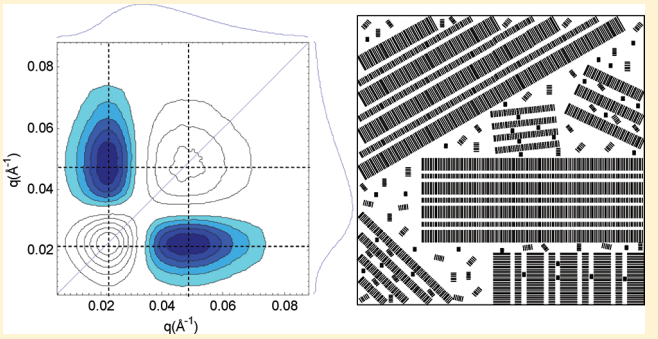

INTRODUCTION

The physical properties of semicrystalline polymeric materials are ultimately dictated by their morphology in the solid state. This morphology is a complex function of molecular characteristics and thermal and flow history. To improve control over the morphology, and hence material properties, ongoing research examines transient morphological development using techniques such as wide-angle and small-angle X-ray scattering (WAXS and SAXS, respectively).[1−6] Conventional analyses of time-resolved scattering data focus on a few particular characteristics, such as peak location or relative peak area. Rich information regarding the complex evolution of morphology during crystallization that is contained in X-ray scattering curves as a whole has proven more difficult to analyze and communicate. Here, we apply two-dimensional (2D) correlation analysis methods to discern important structural changes that occur during crystallization. In the field of vibrational spectroscopy, 2D correlation analysis has proven to be a powerful method to analyze the sometimes subtle changes in spectral intensities in protein, liquid crystal, and polymer systems in response to a perturbation variable (e.g., temperature) (see review by Noda[7]). However, its application to other experimental probes, such as synchrotron X-ray data, has been surprisingly limited.[8,9]

Model ethylene copolymers are used to illustrate 2D correlation analysis of WAXS and SAXS patterns. The results provide characteristic fingerprints of distinct morphological regimes during nonisothermal crystallization. Prior literature identifies two crystallization regimes based on conventional X-ray analyses: (1) "irreversible" crystallization and melting is characterized by the expected hysteresis and large changes in crystallinity and other morphological parameters and is observed at elevated temperatures; (2) "reversible" crystallization and melting observed at lower temperatures exhibits negligible hysteresis and relatively small changes in morphological parameters during cooling and subsequent heating.[2,10−14] The present application of 2D correlation analysis indicates that a third regime should be distinguished. During cooling, the physics of irreversible crystallization crosses over from propagation of primary lamellae into unconstrained melt to nucleation and growth of secondary lamellae in noncrystalline material that is constrained by previously formed crystallites. Therefore, we refer to three regimes of crystallization in copolymers: primary-irreversible, secondary-irreversible, and reversible crystallization. In addition to providing fingerprints of the primary- and secondary-irreversible regimes, 2D correlation analysis shows promise for detection of

Received: April 11, 2011
Revised: June 29, 2011
Published: August 15, 2011

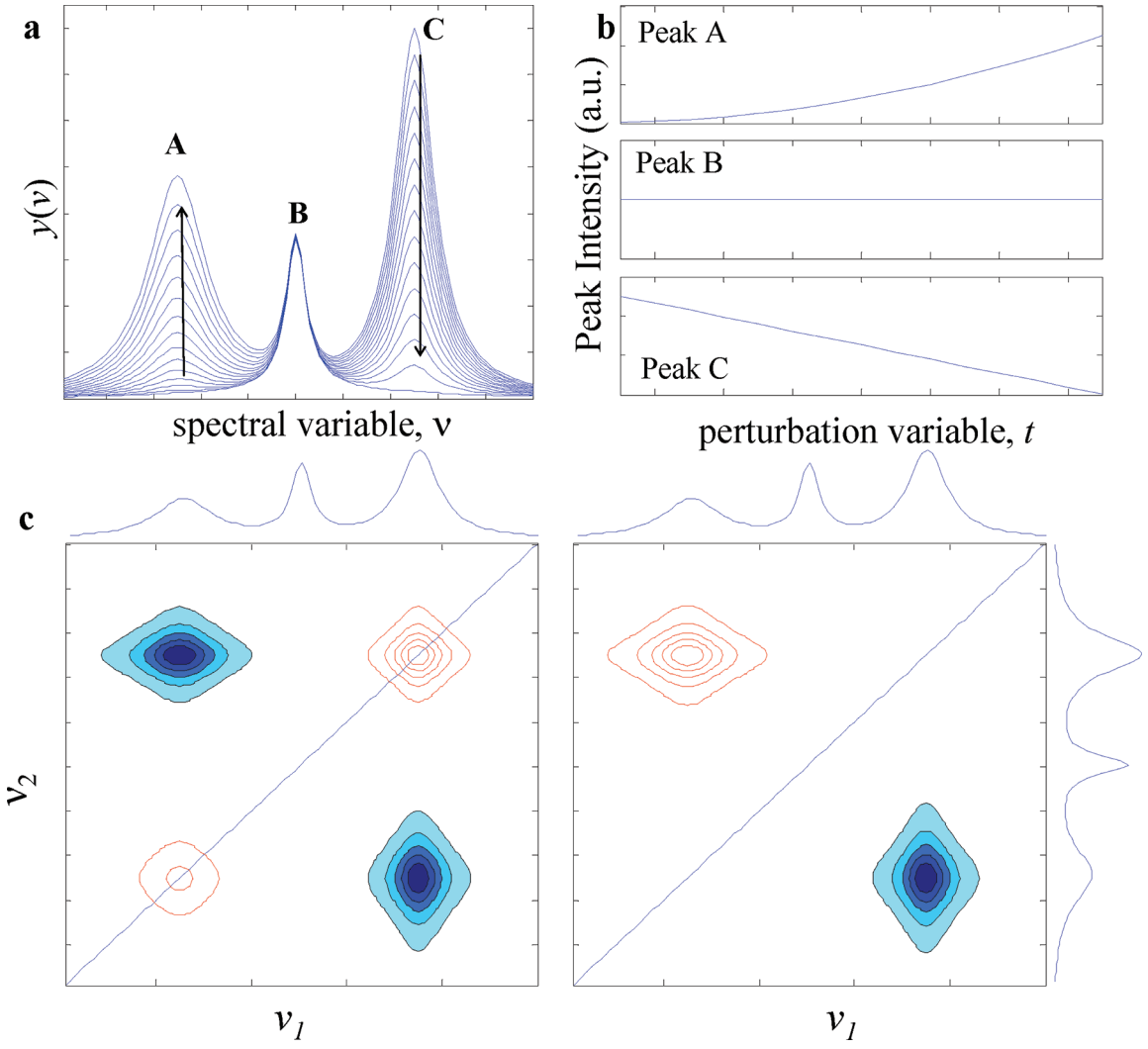

Figure 1. (a) Simulated data set. (b) Evolution of peak intensities with perturbation of peaks in (a). (c) Synchronous (left) and asynchronous (right) 2D correlation plots with perturbation-averaged 1D patterns above and beside. Shaded-in contours are negative, while nonshaded contours are positive.

subtle changes associated with the formation of fringed micelles that form in the reversible crystallization regime.

Two-Dimensional Correlation Analysis. Generalized 2D correlation analysis highlights relationships between intensity changes observed at two different spectral variables, ν_1 and ν_2, as a function of an external perturbation, t. Here, the intensity $y(\nu)$ is that of the scattered X-rays, rather than a spectral absorption or emission; the structural variables are wavevectors, q, rather than wavelengths or frequencies encountered in the spectroscopy literature. A diversity of perturbation variables have been examined in the spectroscopy literature, including strain, temperature, applied electric/magnetic field, irradiation, and time (see review by Noda[7]). The external perturbation is varied over a range of interest, $T_{min} \leq t \leq T_{max}$, and a series of intensity patterns, $y(\nu,t)$, are acquired at different values of the perturbation parameter, t. To emphasize the changes in $y(\nu,t)$ as a function of t, an appropriate reference pattern is subtracted from each spectrum, e.g., the perturbation-averaged pattern, $\langle y(\nu)\rangle$:

$$\tilde{y}(\nu,t) = \begin{cases} y(\nu,t) - \langle y(\nu)\rangle & \textit{for } T_{min} \leq t \leq T_{max} \\ 0 & \textit{otherwise} \end{cases} \quad (1)$$

where $\tilde{y}(\nu,t)$ are referred to as "dynamic spectra" and

$$\langle y(\nu)\rangle = \frac{1}{T_{max} - T_{min}} \int_{T_{min}}^{T_{max}} y(\nu,t)\, dt \quad (2)$$

For illustration a simulated data set (Figure 1a) is constructed with peaks that increase quadratically (peak A), decrease linearly (peak C), or remain unchanged (peak B) as the perturbation parameter is varied (Figure 1b). The average of these spectra $\langle y(\nu)\rangle$ (shown on the sides of Figure 1c) serves as the reference and is subtracted from each individual spectrum to obtain the set of dynamic spectra (not shown).

Synchronous correlation analysis highlights pairs of ν-values that exhibit simultaneous or coincidental changes in intensity in response to the perturbation. The 2D synchronous correlation

$$\Phi(\nu_1,\nu_2) = \frac{1}{T_{max} - T_{min}} \int_{T_{min}}^{T_{max}} \tilde{y}(\nu_1,t)\cdot\tilde{y}(\nu_2,t)\, dt \quad (3)$$

which is the perturbation-averaged outer product of $\tilde{y}(\nu,t)$ is symmetric by definition. The diagonal of the 2D synchronous correlation plot is the autocorrelation intensity (always positive);

Table 1. Noda's Rules for Sequential Order When $\nu_1 > \nu_2$

$\Phi(\nu_1,\nu_2)$	$\Psi(\nu_1,\nu_2)$	interpretation
+	+	ν_1 precedes ν_2
+	−	ν_1 lags ν_2
−	+	ν_1 lags ν_2
−	−	ν_1 precedes ν_2

thus, $\Phi(\nu,\nu)$ represents the total magnitude of the intensity variation in response to the perturbation.

In the above example, peaks A and C each give rise to positive "autopeaks" along the diagonal of $\Phi(\nu_1,\nu_2)$ (Figure 1c, left). The 2D correlation analysis filters out static features, so peaks that remain unchanged (such as peak B) are absent from the 2D pattern. Off-diagonal peaks occur at coordinates (ν_1,ν_2) at which both intensities $y(\nu_1,t)$ and $y(\nu_2,t)$ change with t. Specifically, positive peaks in $\Phi(\nu_1,\nu_2)$ indicate $y(\nu_1,t)$ and $y(\nu_2,t)$ both change in the same direction, and negative extrema indicate they change in opposite directions, as is the case with peaks A and C (Figure 1c, left).

Asynchronous correlation analysis is used to characterize the extent to which one change precedes (or lags behind) another. For this purpose, it is useful to generalize the concept of oscillatory responses that are out of phase with (i.e., orthogonal to) one another. When the perturbation parameter varies in a nonperiodic manner, Noda utilized the Hilbert transform of $\tilde{y}(\nu,t)$ with respect to t to obtain an orthogonal function $\tilde{z}(\nu,t)$.[15−17] The extent to which the response at ν_1 is orthogonal to that at ν_2 is quantified by the perturbation-averaged outer product of $\tilde{y}(\nu,t)$ with $\tilde{z}(\nu,t)$:

$$\Psi(\nu_1,\nu_2) = \frac{1}{T_{\max} - T_{\min}} \int_{T_{\min}}^{T_{\max}} \tilde{y}(\nu_1,t)\cdot\tilde{z}(\nu_2,t)\,\mathrm{d}t \qquad (4)$$

where

$$\tilde{z}(\nu,t) \equiv \frac{1}{\pi}\,{}_{Pv}\int_{-\infty}^{\infty} \frac{\tilde{y}(\nu,t)}{t'-t}\,\mathrm{d}t' \qquad (5)$$

and ${}_{Pv}\int$ represents the implementation of the Cauchy principal value such that the singularity at $t = t'$ is excluded from the integration. The numerical method that is used to compute $\tilde{z}(\nu,t)$ from experimental data is described below.

The sign of the cross-peaks in the asynchronous pattern reveals the sequential order of peak variations based on Noda's rules.[16,18] Interpretation of the sign of a cross-peak in the asynchronous plot depends on the sign of the corresponding cross-peak in the synchronous plot. Since $\Psi(\nu_1,\nu_2)$ is antisymmetric, it suffices to identify the sign of the cross-peak in the region $\nu_1 > \nu_2$ (below the diagonal). If $\Phi(\nu_1,\nu_2)$ is positive, then a positive asynchronous cross-peak below the diagonal indicates that the response at ν_1 precedes that at ν_2; if $\Phi(\nu_1,\nu_2)$ is negative, then that positive cross-peak in $\Psi(\nu_1,\nu_2)$ indicates that the response at ν_1 lags that at ν_2 (Table 1).

In the example above, the 2D asynchronous correlation plot (Figure 1c, right) contains no diagonal peaks, in accord with its antisymmetric nature. Two off-diagonal features indicate that the intensity changes of peaks A and C vary differently with t (quadratic vs linear, see Figure 1b). In both the synchronous and asynchronous ($\nu_1 > \nu_2$) plots, the cross-peaks corresponding to peaks A and C are negative. Therefore, the change in peak C precedes that in peak A. This temporal separation can be practically interpreted as a difference in half-intensity and half-time of peak evolution.[19] Indeed, from Figure 1b, it is apparent that peak C achieves half of its total intensity change earlier in the perturbation than peak A.

The abundant application of 2D correlation spectroscopy has led to further developments,[7] including heterocorrelation analyses of two independent measurements of perturbation-induced dynamic spectra. Most frequently, heterospectral correlation is applied to two different spectral probes; here, it will be applied to small- and wide-angle X-ray scattering.

The application of 2D correlation analysis provides distinct advantages that can be utilized to extract information about morphology from X-ray scattering data during crystallization or melting: deconvolution of overlapping features, determination of sequential order of intensity changes, and enhancement of spectral resolution by spreading data over a second dimension. Additionally, heterospectral correlation analysis[16] allows one to directly visualize changes in SAXS and WAXS that are the result of the same physical processes.

Unresolved Issues in Copolymer Crystallization. The specific example of ethylene copolymers illustrates how correlation analysis can provide new insights into long-standing debates. Understanding of ethylene copolymer crystallization has proven elusive, as even their degree of crystallinity from WAXS is difficult to characterize. There has been significant debate regarding reasons for poor results of the calculated crystallinity from conventional X-ray analysis of WAXS curves fitted using a two-phase model: one peak for the amorphous halo and one peak for each of the crystalline reflections.[3−5,20−24] Fitting the amorphous halo with two peaks sometimes yields a better fit and more reasonable behavior of all peaks considered (position, width, etc.).[3−5,20,21,24] However, the physical justification of this additional peak is controversial. Observation of a hexagonal mesophase in some studies[25−27] was not corroborated in others.[14,20,21,28,29] Alternatively, one or more peaks have been proposed to account for a "semiordered", "transition", or "intermediate" phase/region. Simanke et al. reject this possibility, arguing that scattering from conformationally diffuse interfacial regions would not be limited to any particular angular region in the WAXS patterns.[20] Nonetheless, some groups maintain the existence of a semiordered phase that contributes one or two relatively narrow reflections. Sajkiewicz et al.[4] envision a phase with structure intermediate between crystalline and amorphous that contributes a hidden, relatively narrow peak between the amorphous halo and the (110) reflection. When two peaks have been attributed to the putative semiordered region, they have closely resembled the (110) and (200) orthorhombic reflections, but weaker in intensity and shifted to lower q-values.[5,21,22,24] These are referred to as "(110)" and "(200)", respectively, by Rabiej et al.[22] An alternative explanation for the poor fit provided by the two-phase model is that a possible transition region between the crystalline and noncrystalline layers contributes to density heterogeneity which can be captured by an additional amorphous-halo-like scattering in a large angular range.[3,23] Correlation analysis is well-suited to discriminate among these competing hypotheses by resolving overlapping features and identifying multiple features that arise from the same underlying physical processes.

In the following, we examine the evolution of morphology during the crystallization of a random copolymer using synchronous, asynchronous, and heterospectral 2D correlation analyses. Distinguishing features of different morphologies (primary and secondary lamellae, fringed micelles) and physical processes

(crystal growth, thermal contraction, etc.) are identified. The results provide insight into the complex crystallization behavior of polyethylenes containing short-chain branches.

EXPERIMENTAL METHODS

Materials. In the current work, we examine a linear hydrogenated polybutadiene of molecular weight M_w = 152 kg/mol denoted L152, synthesized using anionic polymerization and subsequent hydrogenation protocols described previously.[30] This synthetic approach confers low polydispersity (M_w/M_n < 1.05) and random short chain branch (SCB) distribution.[30−33] L152 is equivalent to an ethylene-*co*-butene with 19.5 branches per 1000 backbone carbon atoms determined by solid-state NMR.

X-ray Scattering. Morphology development during controlled heating and cooling at 10 °C/min between 0 and 160 °C in an INSTEC STC200 hot stage was monitored using wide- and small-angle X-ray scattering (WAXS and SAXS, respectively) at beamline X27C of the National Synchrotron Light Source (NSLS, Brookhaven National Lab, Upton, NY) with a wavelength, λ, of 1.371 Å.[34] A MARCCD detector with 158 μm pixel size was used to record one two-dimensional scattering pattern with a 7 s collection time every 2 °C during the ramp, resulting in 5 frames/min. Samples were placed between Kapton tape into a holder with 0.5 cm diameter and 1.558 mm thickness. Following experiments, samples were examined to ensure to significant change in thickness was observed.

X-ray data pretreatment included the subtraction of the background and adjustment for incident X-ray beam flux and acquisition time. The azimuthally averaged intensity was extracted as a function of scattering vector, $q = 4\pi \sin(\theta)/\lambda$, where θ is the scattering angle. Since the samples were isotropic, a Lorentz correction[35] was applied by multiplying the scattering intensity, $I(q)$, by the square of scattering vector, q: $J(q) = I(q)q^2$.

The SAXS long period, L_p, was determined from the position of the peak in $J(q)$, q_{max}, as $L_p = 2\pi/q_{max}$. The area under the Lorentz-corrected SAXS intensity curve (for isotropic samples) in the full range of q ($0 < q < \infty$) defines the invariant, which is a measure of the total scattering power of the sample. Given the experimental constraints, we approximate the invariant by the integrated intensity, Q, in the range available ($q_{min} < q < q_{max}$):

$$Q = \int_{q_{min}}^{q_{max}} q^2 I(q)\, dq \tag{6}$$

The WAXS crystallinity index, X_c, was determined as the ratio of the area of the crystalline peaks, A_c, to the combined area of the amorphous halo, A_a, and the crystalline peaks: $X_c = A_c/(A_a + A_c)$. Areas were obtained after fitting the amorphous halo and the orthorhombic crystal reflections due to the (110) and (200) planes with Lorentzian functions using Origin 7.5.

Computation: 2D Correlation Analysis. *Synchronous and Asynchronous.* Two-dimensional (2D) correlation spectra were calculated using Noda's generalized method[15,36] from a discrete set of Lorentz-corrected scattering curves measured at m equally spaced temperatures during a temperature ramp:

$$J_i(q) = J(q, T_i) \qquad i = 1, 2, 3, \ldots, m \tag{7}$$

The discrete dynamic spectra, $\tilde{J}(q,T_i)$, were calculated with respect to a temperature-averaged spectrum, $\langle J(q)\rangle$:

$$\tilde{J}(q, T_i) = J(q, T_i) - \langle J(q)\rangle \qquad i = 1, 2, 3, \ldots m \tag{8}$$

$$\langle J(q)\rangle = \frac{1}{m}\sum_{i=1}^{m} J(q, T_i) \tag{9}$$

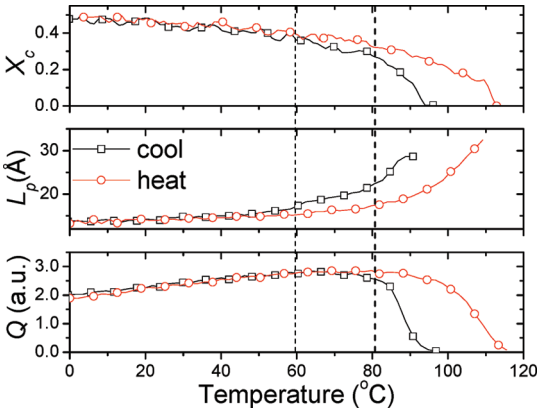

Figure 2. Evolution of WAXS crystallinity, X_c, SAXS long period, L_p, and SAXS scattering power, Q, during cooling and subsequent heating of L152 with three crystallization regimes marked. Data points are spaced 2 °C apart.

The synchronous 2D correlation intensity, demonstrating simultaneous or coincidental changes in intensity, is given by

$$\Phi(q_1, q_2) = \frac{1}{m-1}\sum_{i=1}^{m} \tilde{J}_i(q_1)\cdot\tilde{J}_i(q_2) \tag{10}$$

The asynchronous 2D correlation spectra, showing changes in intensity that lag/lead one another, is given by

$$\Psi(q_1, q_2) = \frac{1}{m-1}\sum_{i=1}^{m} \tilde{J}_i(q_1)\cdot\tilde{z}_i(q_2) \tag{11}$$

where $\tilde{z}_i(q_2)$ are the discrete orthogonal spectra. We use the approximation introduced by Noda[16] that permits $\tilde{z}_i(q_2)$ to be expressed in terms of a linear transformation of discrete dynamic spectra, $\tilde{J}_i(q_2)$

$$\tilde{z}_i(q_2) = \sum_{j=1}^{m} N_{ij}\cdot\tilde{J}_j(q_2) \tag{12}$$

where N_{ij} is the Hilbert−Noda transformation matrix

$$N_{ij} = \begin{cases} 0 & \text{if } i = j \\ \dfrac{1}{\pi(j-i)} & \text{otherwise} \end{cases} \tag{13}$$

Heterospectral Correlation Analysis. Simultaneous changes in SAXS and WAXS that arise from the same underlying physical processes are revealed by 2D heterospectral correlation analysis. The synchronous 2D heterospectral correlation spectrum identifies simultaneous changes in the system observed by two different probes in response to the same perturbation: Lorentz-corrected SAXS ($J_{SAXS,i}(q) = J_{SAXS}(q,T_i)$, i = 1, 2, 3, ..., m) and WAXS ($J_{WAXS,i}(q) = J_{WAXS}(q,T_i)$, i = 1, 2, 3, ..., m) curves collected during temperature ramps. Specifically, the "2D het-corr" pattern is calculated from the dynamic 1D patterns (eq 8) as

$$\Phi(q_1, q_2) = \frac{1}{m-1}\sum_{i=1}^{m} \tilde{J}_{SAXS,i}(q_1)\cdot\tilde{J}_{WAXS,i}(q_2) \tag{14}$$

For image presentation, contour levels were adjusted to exclude the lower 5% of intensity values. Additionally, contour plots reveal relative intensities; therefore different figures have different contour levels in order to highlight the relevant features in each case. Unless otherwise stated, intensity values between different figures should not be compared by the apparent relative intensity of features.

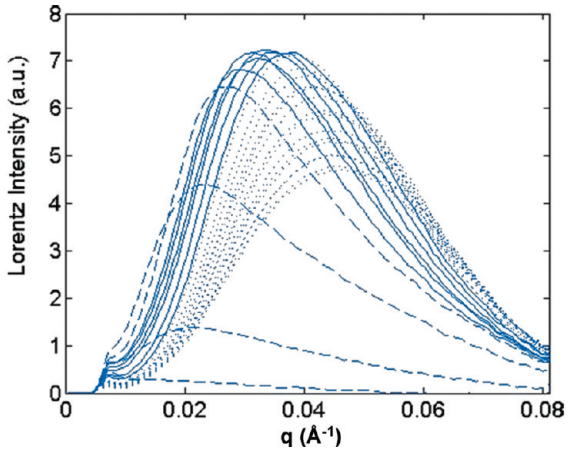

Figure 3. Lorentz-corrected SAXS of L152 during cooling at 10 °C/min exhibiting primary-irreversible (dashed lines), secondary-irreversible (solid lines), and reversible (dotted lines) regimes.

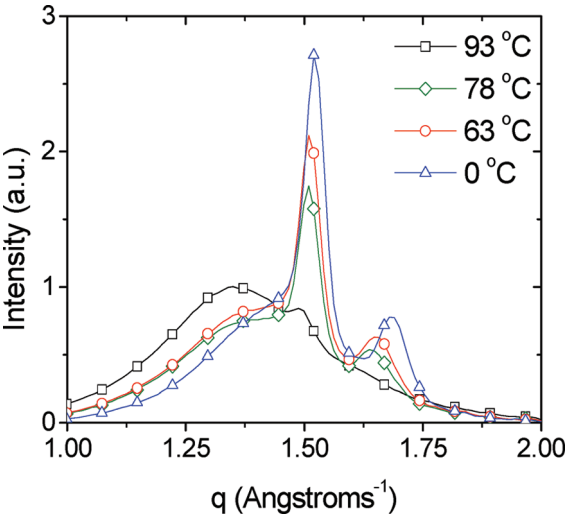

Figure 4. WAXS intensity during cooling at 10 °C/min at temperatures marking the bounds of different crystallization regimes L152 while cooling at 10 °C/min.

RESULTS AND DISCUSSION

Evolution of Conventional Morphological Parameters. During quiescent cooling (heating) ramps of L152, the crystallinity, X_c, long period, L_p, and SAXS integrated intensity, Q, exhibit two well-established regimes as seen in prior literature for SCB materials:[2,10−14] irreversible and reversible crystallization (melting). The irreversible crystallization regime exhibits the usual hysteresis upon cooling and heating (Figure 2, $T > 60$ °C) and is marked by relatively large changes in morphological parameters (L_p, X_c and Q). The reversible crystallization regime is defined by the absence of hysteresis, i.e., morphological parameters during cooling and subsequent heating overlap (Figure 2, $T < 60$ °C).

However, closer evaluation of the evolution of morphological parameters reveals that the irreversible crystallization regime of this model random copolymer can be further divided into two regimes: the "primary-irreversible" crystallization regime (Figure 2, $T > 80$ °C) in which large changes in the morphological parameters occur with profound hysteresis in all three (X_c, L_p, and Q); the "secondary-irreversible" crystallization regime (between the two dashed lines in Figure 2), characterized by gradual changes and mild hysteresis in X_c and L_p and nearly constant Q. Similar observations were made for other HPBD and metallocene systems and can be found in literature.[2,10−12,14]

The three regimes of crystallization reproducibly exhibited by HPBD materials (see ref 17) are apparent in the evolution of Lorentz-corrected SAXS curves during cooling of L152 (Figure 3). Irreversible crystallization at high temperatures (primary-irreversible regime, dashed lines in Figure 3) is characterized by an overall increase in the scattering power and a shift in the peak position to larger values of q. At intermediate temperatures (secondary-irreversible regime, solid lines in Figure 3), overall scattering power stays relatively constant while the peak position continues its shift. In the reversible regime at lower temperatures (dotted lines in Figure 3), the overall SAXS power decreases while the peak position further shifts and broadens. Note that in each regime the change in the peak position and shape (magnitude and width) is monotonic, enabling the application of Noda's rules for sequential order determination (Table 1).[18]

Primary-irreversible crystallization is manifested in WAXS by an increase in crystalline material at the expense of amorphous material (between 93 and 78 °C, Figure 4); over half of the crystallinity that is present in the sample at the lowest temperature examined (0 °C) forms in the primary-irreversible regime. Secondary-irreversible crystallization (between 78 and 63 °C in Figure 4) results in further increase of crystalline material without appearing to consume amorphous material: the amorphous halo remains largely unchanged and even increases near $q = 1.38$ Å^{-1}. During reversible crystallization, which occurs over a very broad temperature range from 63 °C down to the lowest temperature examined, diffraction peaks grow in intensity and the amorphous halo decreases (but only at $q < 1.38$ Å^{-1}).

The succession of regimes reflects the cascade of crystallization processes that occur during cooling. Crystallites that grow early in the process impose constraints on subsequent growth, leading to the formation of primary lamellae, secondary lamellae, fringed micelles, and "rigid amorphous" material. The motivation for applying 2D correlation analysis to the WAXS and SAXS results for these three regimes is to elucidate how these processes interrelate and influence one another.

Primary-Irreversible Crystallization. The simplest of the three regimes is the initial growth of primary lamellae into unperturbed, subcooled melt. The 2D correlation patterns for this regime provide a point of departure for comparison to subsequent growth regimes.

SAXS. The synchronous SAXS correlation plot during primary-irreversible crystallization is dominated by the monotonic increase in scattering power throughout the q-range examined (Figure 5, top left). Along the diagonal, the autocorrelation function has a single, broad peak near the position evident in the average scattering curve, indicative of lamellar stacks with a broad distribution of long periods centered near 22 nm. The triangular shape of this peak reflects the asymmetric shape of the SAXS peak (steeper on the low-q side than the high-q side, Figure 3). The asynchronous plot (Figure 5, top right) indicates that, in this regime, the intensity of the peak increases first at low q and then later at high q. Specifically, the negative peak below the diagonal centered at (0.017 Å^{-1}, 0.031 Å^{-1}) indicates that the broad distribution of long periods arises through the initial formation of lamellar stacks with an average long period of ~37 nm, followed by

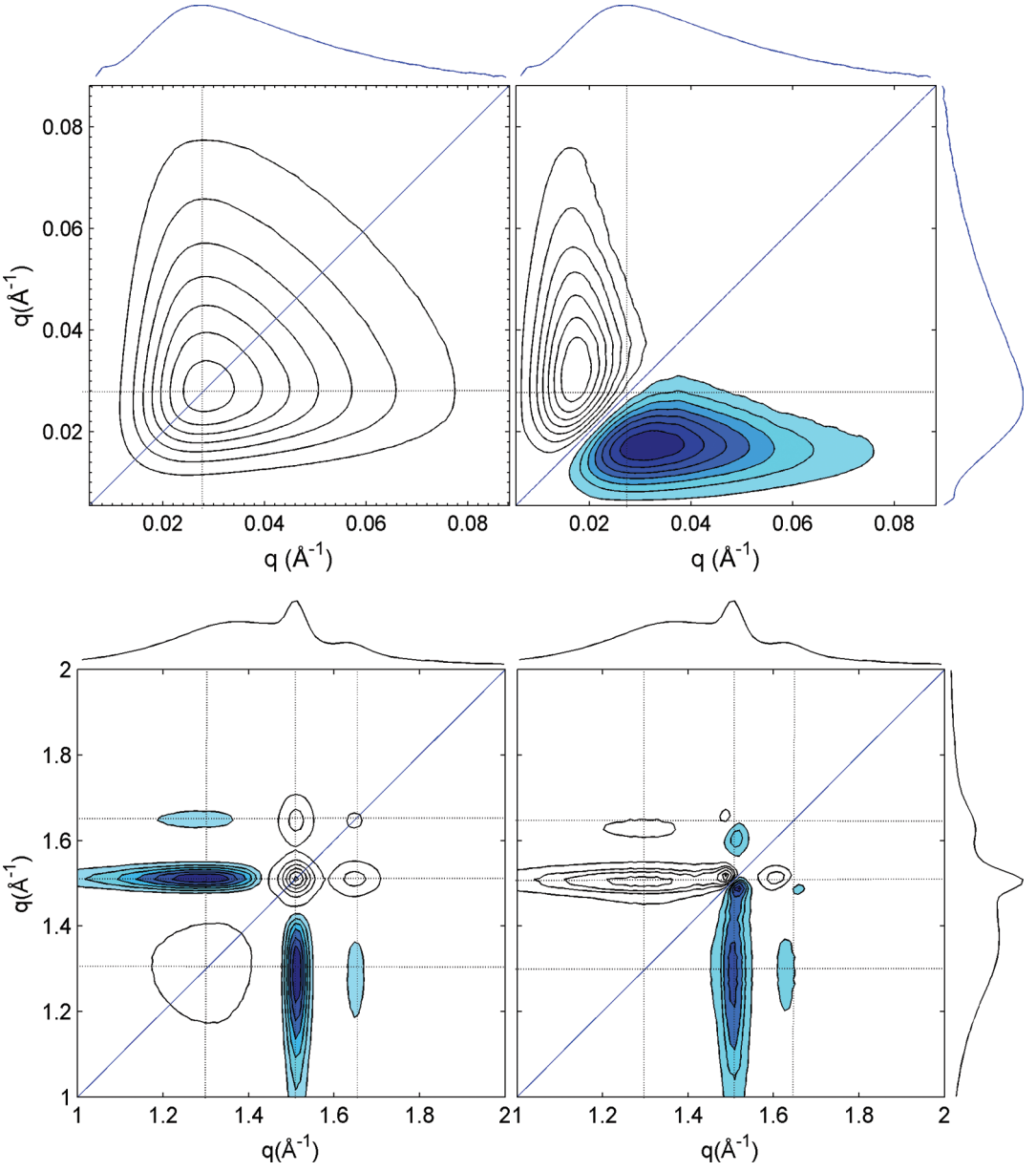

Figure 5. 2D synchronous (left) and asynchronous (right) correlation plots computed from Lorentz-corrected SAXS (top) and WAXS (bottom) curves collected during primary-irreversible crystallization of L152 (78 °C < T < 93 °C). Positive and negative contours are shown as open and filled, respectively. Averaged 1D scattering profiles acquired in this temperature range are shown on the sides. The dotted lines in the SAXS correlation plots are at 0.028 $Å^{-1}$, and those in the WAXS plots are at 1.30, 1.51, and 1.65 $Å^{-1}$ (see text).

the formation of lamellae that lead to lamellar stacks with long spacing of ~20 nm.

A strictly positive change in scattering intensity at all q values as temperature decreases from 93 to 78 °C is consistent with the formation of *primary lamellae* propagating into unconstrained melt (hence, the choice of name for this regime). The relatively fast growth of crystallites into unperturbed melt is consistent with the steep rise of crystallinity in the primary-irreversible regime (Figure 2). The formation of lamellar stacks with progressively smaller long spacing is a consequence of both the nonisothermal conditions and the ethylene sequence length distribution (ESLD). The first lamellae to form during cooling preferentially incorporate the longest ethylene sequences.[37] Because of the homogeneous SCB distribution in the present hydrogenated polybutadiene, virtually every chain includes some long ethylene sequences; in fact, for these polymers, one can calculate that there are two or more sequences of 115 ethylenes (330 methylenes) in every chain.[38−40] However, these represent the minority of each chain and of the melt as a whole. The crystallization of these long sequences leaves the majority of each participating chain dangling in the adjacent melt. By this reasoning, the early lamellar stacks are expected to have noncrystalline layers that are much thicker than their crystalline lamellae. It is quite plausible that the majority of chains in these noncrystalline layers may be pinned to crystal surfaces, frustrating their ability to participate in the nucleation and growth of further lamellae; a substantially deeper subcooling might be required to induce their crystallization (see below).

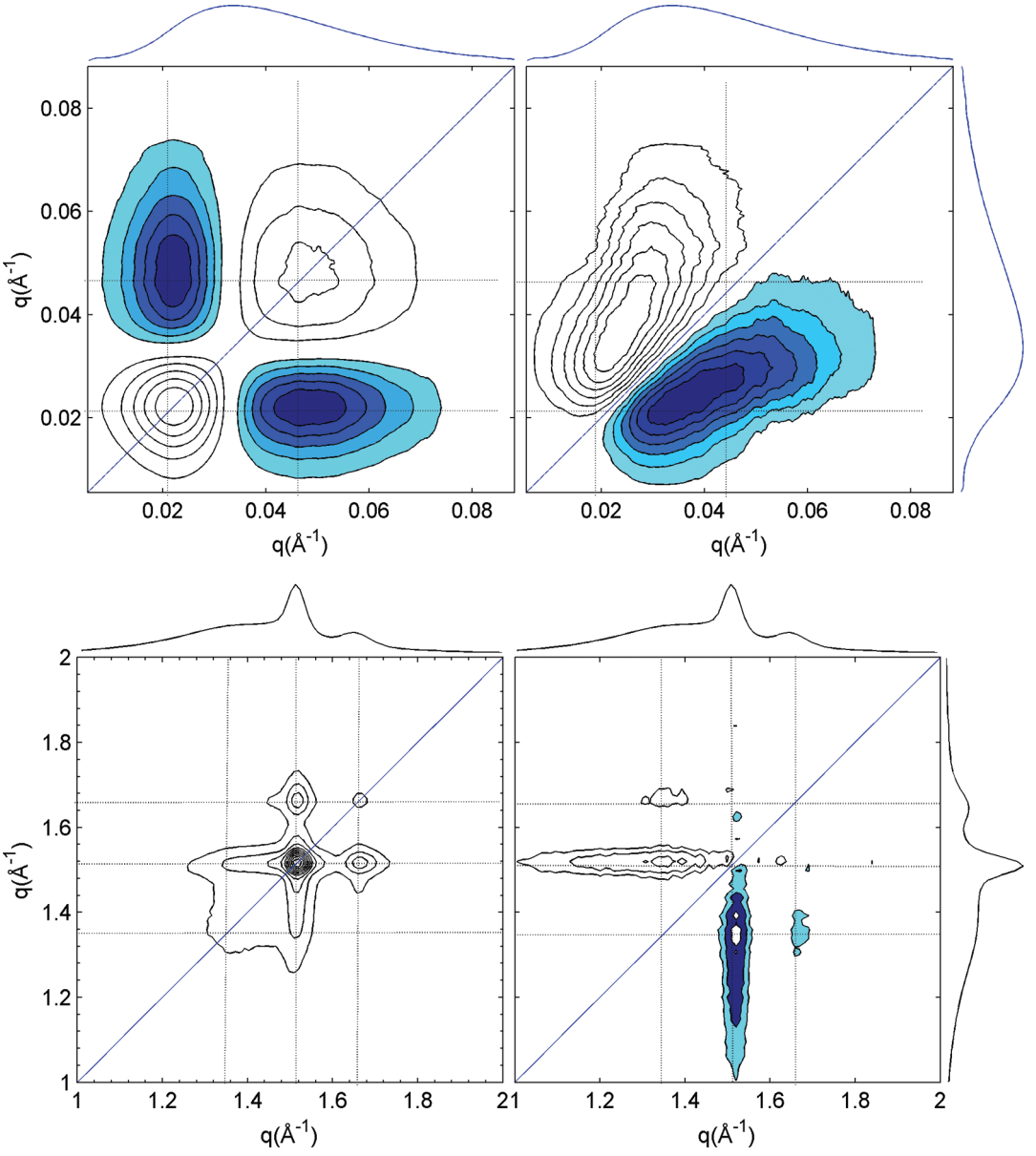

Figure 6. 2D synchronous (left) and asynchronous (right) correlation plots computed from Lorentz-corrected SAXS (top) and Lorentz-corrected WAXS (bottom) curves collected during cooling at 10 °C/min in the secondary-irreversible crystallization regime of L152 (63 °C < T < 78 °C). Positive and negative contours are shown as open and filled, respectively. Averaged 1D scattering profiles are shown on the sides. The dotted lines in the SAXS correlation plots are at 0.022 and 0.048 Å^{-1}; those in the WAXS plots are at 1.35, 1.51, and 1.66 Å^{-1} (see text).

As temperature decreases, thinner primary lamellae nucleate and grow into the remaining unconstrained melt, allowing progressively shorter ethylene sequences to participate. Since a larger percentage of each polymer chain is able to crystallize at lower temperatures, the noncrystalline layers in the resulting primary lamellar stacks may be progressively closer to the thickness of the crystalline lamellae. The progressively smaller long period of the lamellar stacks that form in the primary-irreversible regime is consistent with both thinner crystallites and smaller content of noncrystalline material in the lamellar stack.

WAXS. Analysis of the WAXS two-dimensional correlation plots focuses on three salient features of polyethylene: the broad amorphous halo (centered at ~1.3 Å^{-1}) and the two most prominent crystalline reflections of the orthorhombic unit cell, which are due to the (110) planes (near 1.5 Å^{-1}) and the (200) planes (near 1.65 Å^{-1}). The WAXD 2D synchronous pattern (Figure 5, bottom left) exhibits three autopeaks (along the diagonal) at approximately 1.3, 1.5, and 1.65 Å^{-1}. Furthermore, since the intensities of the three peaks change as the result of the same physical process—the formation of orthorhombic unit cells—strong cross-peaks are observed. The cross-peaks between the (110) and (200) crystalline reflections at (1.51 Å^{-1}, 1.65 Å^{-1}) are positive because both peaks change in the same direction (i.e., both increase). In contrast, the cross-peaks between the crystalline reflections and the amorphous halo, centered at approximately (1.51 Å^{-1}, 1.30 Å^{-1}) and (1.65 Å^{-1}, 1.30 Å^{-1}), are negative due to the opposite direction of changes in intensity of the amorphous halo compared with the crystalline reflections.

The faint features in the asynchronous plot (Figure 5, bottom right) can be attributed to shifting of the crystalline and

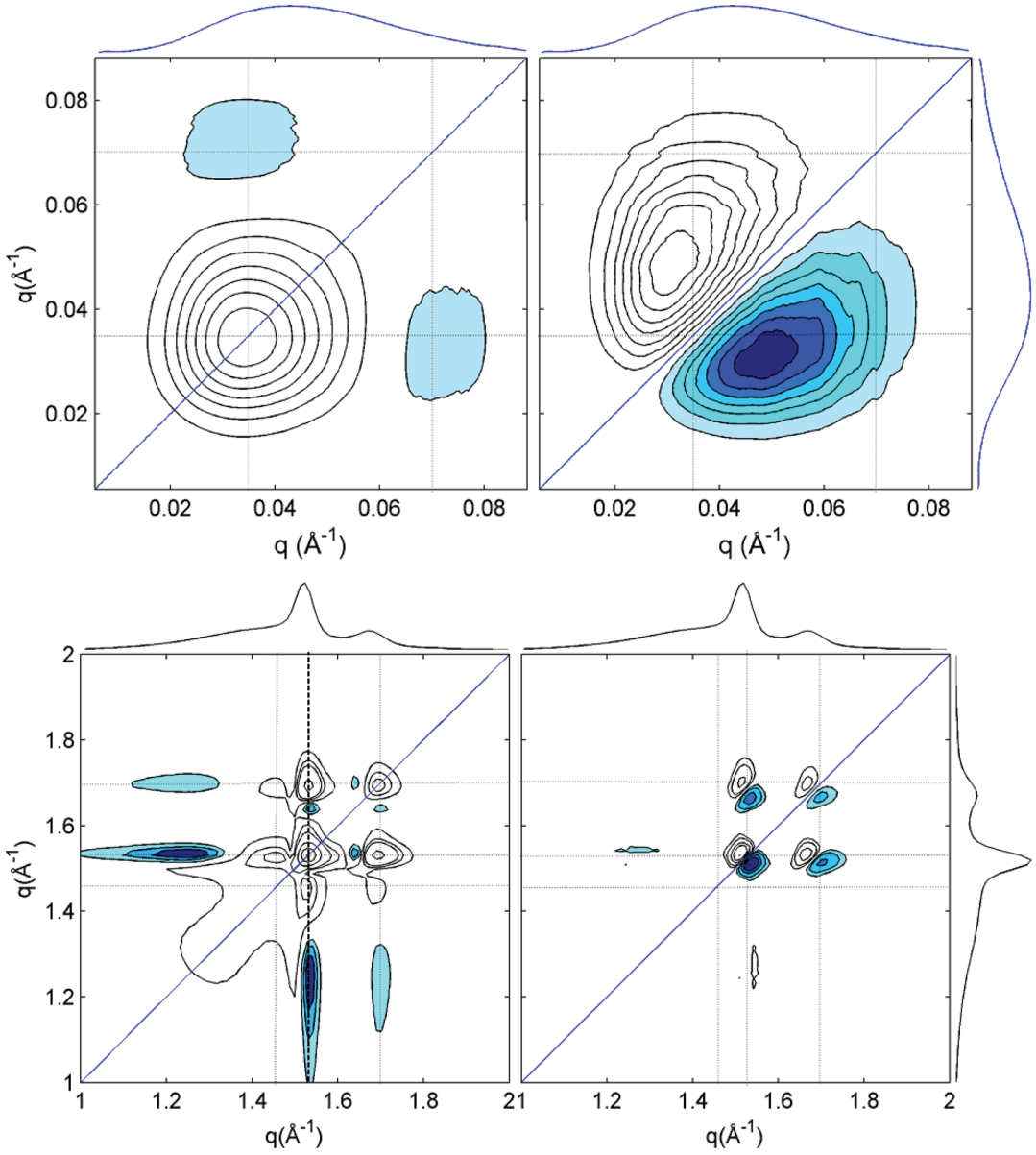

Figure 7. 2D synchronous (left) and asynchronous (right) correlation plots computed from Lorentz-corrected SAXS (top) and Lorentz-corrected WAXS (bottom) curves collected during cooling at 10 °C/min in the reversible crystallization regime (0 °C < T < 63 °C) of L152. Positive and negative contours are shown as open and filled, respectively. Averaged 1D scattering profiles are shown on the sides (also in Figure 8a). The dotted lines in the SAXS correlation plots are at 0.035 and 0.070 Å^{-1}; those in the WAXS plots are at 1.46, 1.53, and 1.70 Å^{-1} (see text). Intensity along the long dash of bottom left is plotted in Figure 8c).

amorphous peak positions due to thermal contraction[41−44] convoluted with changes in the shape of the amorphous halo due to the enrichment of ethyl branches in the noncrystalline regions as they are rejected from the crystals during crystallization of HPBDs. It is important to note that the asynchronous features of L152 are over an order of magnitude smaller than the synchronous ones, indicating increases in the (110) and (200) diffracted intensity are very nearly simultaneous with each other and with the decrease in the amorphous halo. Hence, the dominant process during primary-irreversible crystallization is the development of crystal unit cells.

Secondary-Irreversible Crystallization. In this work, we distinguish two regimes within the irreversible regime identified in prior literature: the distinction between the primary-irreversible regime (above) and the secondary-irreversible regime is manifested in qualitatively different 2D correlation patterns.

SAXS. Rather than a single peak in the synchronous SAXS correlation pattern as temperature decreased from 93 to 78 °C during primary-irreversible crystallization (Figure 5, upper left), there are four peaks in the synchronous SAXS correlation pattern as temperature decreases from 78 to 63 °C during secondary-irreversible crystallization (Figure 6, upper left). The off diagonal peaks are negative and have similar magnitude to the autocorrelation peaks: the loss of scattering power at ∼0.022 Å^{-1} is similar in magnitude to the increase at ∼0.048 Å^{-1}. The asynchronous plot (Figure 6, upper right) exhibits a "butterfly pattern", consistent with a change in peak position; the negative sign of the "wing" below the diagonal indicates that the direction of the peak shift is to larger q values.[16]

Consequently, during secondary-irreversible crystallization, the average long period decreases from 28 to 13 nm. This type of peak shift can be interpreted physically as the formation of secondary lamellae within the noncrystalline regions of previously formed lamellar stacks, particularly in the least constrained (thickest) noncrystalline layers. This lamellar insertion explains the decrease of scattering corresponding to the largest long periods (low q) and increased scattering corresponding to long periods that are approximately half in size (higher q).

WAXS. The synchronous WAXS pattern in the secondary-irreversible regime (Figure 6, lower left) is also qualitatively different from that in the primary-irreversible regime: the prominent autopeak and cross-peaks (Figure 5, lower left) due to the decrease in the amorphous halo in the primary irreversible regime are absent in the secondary-irreversible regime. Instead, increases in intensity occur in both the crystalline reflections and the amorphous halo near the (110) reflection, in the range 1.35−1.46 Å^{-1}. A scattering peak in this region was suggested to correspond to an "intermediate" phase by Sajkiewicz et al.[4] However, this observation is also consistent with increased packing density of a fraction of the noncrystalline regions resulting in a heterogeneous density distribution.[3,23]

The familiar autopeaks and cross-peaks associated with the (110) and (200) crystalline reflections at 1.51 and 1.66 Å^{-1} reflect the increase in crystallinity (13%) in this regime. The peaks in the asynchronous plot (Figure 6, lower right) are again very weak relative to the synchronous ones, indicating that the changes in the amorphous phase coincide with the growth of crystals. Interestingly, although the temperature range of secondary-irreversible crystallization of this polymer is the same as for primary-irreversible crystallization (15 °C), the asynchronous spectrum here lacks the doublets expected due to thermal contraction of crystalline unit cells (compare lower right of Figures 5 and 6). Perhaps the secondary lamellae that form in this temperature regime suffer greater interfacial stress due to the accumulation of SCB at their crystal faces; the resulting increase in the size of their unit cells would offset the contraction of the unit cells of the previously formed primary lamellae.[3,4,20,45−51] The crowding of the ethyl groups near the crystal faces could also account for the increase in noncrystalline scattering on the high-q side of the amorphous peak, particularly its synchronous relationship to growth of the secondary lamellae.

Reversible Crystallization. The reversible crystallization regime (0−63 °C) is marked by a lack of hysteresis in the morphological parameters.

SAXS. The synchronous 2D plot is indicative of a loss in overall intensity in a broad range of q (<0.06 Å^{-1}) and a mild increase at $q \sim 0.07$ Å^{-1}. The decrease in intensity is evident as a broad, prominent autopeak centered at 0.035 Å^{-1} (Figure 7, top left). Just as the single prominent autopeak in Figure 5 reflected the increase of intensity as primary lamellae formed, here the autopeak reflects the loss of intensity as reversible crystallites (fringed micelles) form in the noncrystalline layers of lamellar stacks causing a decrease in the electron density contrast.[2] Weak negative cross-peaks at (0.070 Å^{-1}, 0.035 Å^{-1}) indicate that as intensity decreases near 0.035 Å^{-1}, it simultaneously increases near 0.070 Å^{-1}. The corresponding autopeak (not shown) is hardly above the baseline, speaking to the small change in its intensity. The asynchronous plot (Figure 7, top right) again contains a single feature that is elongated along the diagonal suggesting a mild shift in peak position.[41] On the basis of the sign of the feature below the diagonal, this shift is toward larger values

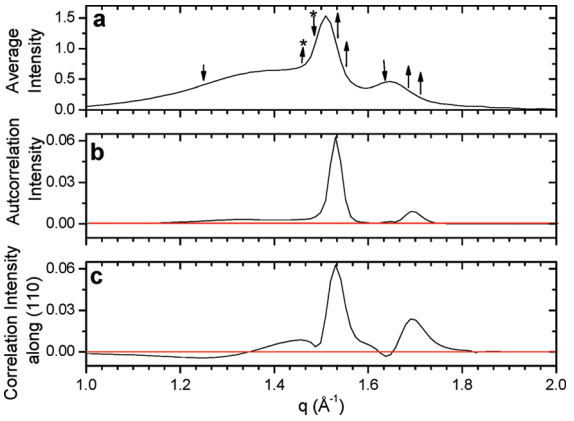

Figure 8. WAXS data for reversible crystallization of L152: (a) average curve with arrows indicating direction of intensity change, (b) intensity along the diagonal of the synchronous plot (Figure 7, bottom left), and (c) synchronous correlation intensity along the (110) reflection marked by long-dashed line in Figure 7, bottom left.

of q (i.e., smaller characteristic length scales).[16] Concurrently with decreasing scattering intensity that is apparent from 1D scattering curves, this slight shift in peak position is consistent with the formation of reversible crystals in the largest noncrystalline regions (corresponding to the largest L_p) first, followed by gradual growth in smaller regions. Additionally, the subtle autopeak at 0.070 Å^{-1} suggests that the reversible crystals have a structural length scale of ∼9.0 nm.

WAXS. The significant increase in crystallinity that is unique to reversible crystallization of L152, and the other HPBDs examined, is apparent in the synchronous plot in the familiar autopeaks corresponding to the (110) and (200) crystalline reflections at (1.53 Å^{-1}, 1.53 Å^{-1}) and (1.70 Å^{-1}, 1.70 Å^{-1}). These peaks are shifted to larger q-values relative to crystallization in the irreversible regimes as a consequence of thermal contraction (Figure 7, bottom left). Thermal contraction continues in the range below 63 °C corresponding to reversible crystallization resulting in the elongated doublets in the asynchronous plot (Figure 7, bottom right). These features are consistent with peak shifting occurring simultaneously with more pronounced changes in intensity.

As discussed previously, all diffraction features shift to higher values of q through a decrease of intensity at low q values and increase of intensity at high q values, which can be seen from 1D WAXS curves at two different temperature in this regime in Figure 4 (at the beginning at T = 63 °C and at T = 0 °C). The autopeaks in the synchronous plot corresponding to the diffraction peaks resemble triangles as a consequence of the increasing breadth of the crystalline reflections, which is the result of crystallization of random copolymers at low temperatures (Figure 4). Increased width of the diffraction peaks results from incoherent growth of unit cells as more chain defects are encountered during crystallization at low temperatures. This effect is manifested as increasing intensity on the right side (high-q side) of the crystalline reflections and corresponding triangular shape of 2D synchronous features. This shape is mirrored by the corresponding cross-peaks since both crystalline reflections change simultaneously.

To further appreciate the richness of the 2D synchronous plot in the reversible regime, it is instructive to consider a selected cross section of the plot. In particular, a section of $I(q_1,q_2)$ holding q_1 constant at the (110) diffraction peak, such that $q_1 = q_{(110)}$ (intensity along long-dashed line in Figure 7, bottom left)

is compared with the temperature-averaged intensity in this regime ($J(q)$, analogous to eq 9; Figure 8a) and the intensity pattern along the diagonal of the 2D synchronous plot referred to as the autocorrelation intensity (Figure 8b). Moving along $q_1 = q_{(110)}$ in Figure 7, bottom left, from high q to low q (Figure 8c) there is a strong positive peak ($q \approx 1.70$ Å^{-1}), a shallow negative interval ($q \approx 1.64$ Å^{-1}), a shoulder leading up to the strong (110) autopeak, a resolved positive peak ($q \approx 1.46$ Å^{-1}), and a broad negative feature ($q < 1.34$ Å^{-1}).

The strongest feature in Figure 8c is due to the (110) autopeak (where the long-dashed line crosses the diagonal in Figure 7, bottom left), confirmed by its correspondence in position and intensity with the peak in the autocorrelation spectrum (Figure 8b). This peak is offset to high q relative to the (110) peak in the average intensity (Figure 8a), since it reflects the increase of intensity during cooling from 63 to 0 °C. This increase occurs mainly on the high-q side of the diffraction peaks (indicated by upward arrows on the high-q side of both diffraction peaks in Figure 8a) due to the simultaneous thermal contraction of previously formed crystallites and the formation of new ones.

The second strongest feature in the correlation intensity along $q_{(110)}$ occurs in a section through the (110)/(200) cross-peak above the diagonal in Figure 7, bottom left, where the dashed line passes through it at 1.70 Å^{-1}. It is readily assigned to the positive correlation between growth of intensity on the high-q side of both the (110) and (200) peaks.

There is a third positive peak in the correlation intensity along $q_{(110)}$ at 1.46 Å^{-1} (Figure 8c). Like the (110)/(200) cross-peak, the positive sign of this peak indicates an increase of intensity at 1.46 Å^{-1} that coincides with the increase in intensity on the high-q side of the (110) peak. Because of both its position and breadth, this feature is attributed to noncrystalline material.

There are also two negative intervals along $q_{(110)}$: a broad one at $q < 1.34$ Å^{-1} and a narrow one at 1.64 Å^{-1}. The former is assigned to the decrease in intensity in the amorphous halo at $q <$ 1.34 Å^{-1} (compare 63 to 0 °C in Figure 4 and observe where the long-dashed line in Figure 7, bottom left, cuts through the elongated negative feature in the synchronous plot). The negative intensity near 1.64 Å^{-1} is attributed to the substantial shift of the (200) reflection to higher q values as a consequence of thermal contraction, resulting in a decrease of intensity on the low-q side of the (200) peak (see downward arrow in Figure 8c at 1.64 Å^{-1}). A similar negative feature is expected on the low-q side of the (110) peak also. Instead, the decrease of the diffracted intensity at 1.49 Å^{-1} due to thermal contraction (manifested by the local minimum in Figure 8c) is offset by the increase of scattered intensity in the broad range around 1.46 Å^{-1} (see arrows marked with asterisks in Figure 8a).

The simultaneous occurrence of the change in noncrystalline scattering as crystallites form suggests that the formation of crystals alters the structure in adjacent noncrystalline material. The effect has negligible time lag (very weak signatures in the asynchronous plot in Figure 7, bottom right), suggesting that the effect is local; as reversible crystals form, they perturb the noncrystalline structure in their immediate vicinity. This is consistent with the physical interpretation of crystallization at low temperatures, which results in excessive crowding of ethyl groups at the crystal surface and increased constraint of the noncrystalline regions compared to higher temperatures.

Searching for a Semiordered Phase. Prior literature has suggested the existence of a semiordered phase that contributes relatively narrow reflections to WAXS in an attempt to improve the calculation of crystallinity from WAXS patterns.[4,5,21,22,24] However, 1D scattering curves have not yet revealed definitive evidence in the form of a resolved feature of such a phase. Here we apply the enhanced resolution of spectral features provided by 2D correlation analysis to search for possible evidence of a semiordered phase. Specifically, we examine all three crystallization regimes (primary-irreversible, secondary-irreversible, and reversible) for features that could be construed as evidence of a semiordered phase. Cross-correlation features in WAXS near 1.61−1.64 Å^{-1} (at the low-q side of the (200) reflection) and near 1.46 and 1.49 Å^{-1} (adjacent to the (110) reflection) are evaluated for potential assignment to the "(200)" and "(110)" semiordered reflections.[22]

WAXS scattering in the three crystallization regimes exhibit (1) increases near 1.49 and 1.61 Å^{-1} during primary-irreversible crystallization, (2) increases near 1.46 and 1.61 Å^{-1} during secondary-irreversible crystallization, and (3) an increase at 1.46 Å^{-1} but a decrease at 1.64 Å^{-1} during reversible crystallization. The shift of the presumed "(110)" peak to lower q between the primary- and secondary-irreversible regimes (1.49 versus 1.46 Å^{-1}, respectively) without a corresponding shift in "(200)" is unexpected if the two features are attributed to a semiordered phase. The opposite changes in intensity of the presumed "(110)" and "(200)" reflections during reversible crystallization is difficult to reconcile with a unified explanation in terms of a distinct, semiordered phase. Thus, the observed changes in the noncrystalline regions of WAXS do not support this hypothesis.

Instead, we favor the interpretation of McFaddin et al.[3] that attributes observed changes in the noncrystalline WAXS during crystallization to density heterogeneities that can arise from well-established physical phenomena (thermal contraction, loss of coherence in unit cell growth of copolymers at low temperatures, and crystallization-induced heterogeneity in the density distribution of adjacent noncrystalline material). In the present HPBDs, crystallization results in the enrichment of rejected ethyl groups in the noncrystalline regions closest to crystal faces. In contrast to HDPE, which crystallizes by chain folding with frequent nearby re-entry of the chain into the crystal, crystallization of HPBDs incorporates "crystalline stems" that are usually delimited by butene units, resulting in strongly reduced probability of nearby re-entry. The crowding of chains at the crystal surface, in addition to localized butene concentration and thermal contraction of these noncrystalline regions, can explain the change in the shape and position of the amorphous halo.[20,23]

SAXS−WAXS Heterospectral Correlation. Correlation analysis is a powerful tool for visualizing the relationships among structural changes taking place on different length scales in response to a given perturbation. In some cases, the heterospectral correlation analysis simply confirms relationships that are evident by inspection of the individual 1D data sets (illustrated here using SAXS and WAXS measurements in the irreversible regimes). In other cases, "het-corr" analysis exposes relationships that would be difficult to discern otherwise (illustrated here by SAXS-WAXS correlation analysis in the reversible regime).

The strong increase in overall SAXS intensity (Figure 3) and development of crystalline reflections in WAXS at the expense of the amorphous halo (Figure 4) in the primary-irreversible regime give rise to three characteristic features in the heterospectral plot (Figure 9); each of the WAXS features (amorphous halo and two

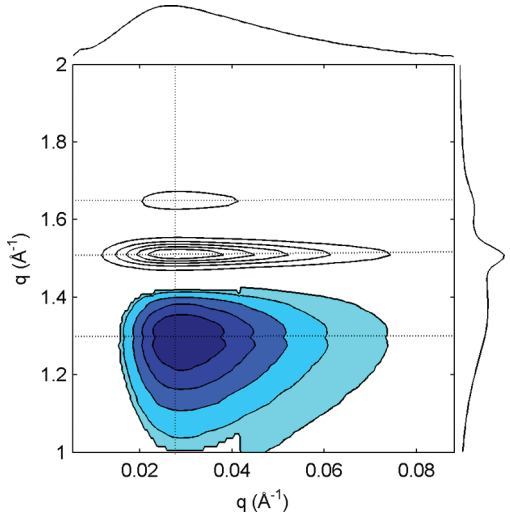

Figure 9. 2D heterospectral correlation plot computed from Lorentz-corrected SAXS and WAXS (horizontal and vertical axes, respectively) during primary-irreversible crystallization of L152. Positive and negative contours are shown as open and filled, respectively. Averaged 1D scattering profiles are shown on the sides. The dotted lines on the SAXS axis are at 0.028 $Å^{-1}$, and those on the WAXS axis are at 1.30, 1.51, and 1.66 $Å^{-1}$ (see text).

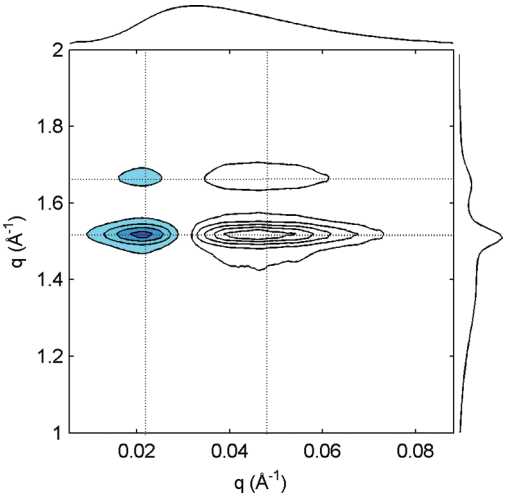

Figure 10. 2D heterospectral correlation plots computed from Lorentz-corrected SAXS and WAXS (horizontal and vertical axes, respectively) during secondary-irreversible crystallization of L152. Positive and negative contours are shown as open and filled, respectively. Averaged 1D scattering profiles are shown on the sides. The dotted lines on the SAXS axis are at 0.022 and 0.048 $Å^{-1}$; those on the WAXS axis are at 1.51 and 1.66 $Å^{-1}$ (see text).

crystalline reflections) is correlated with the SAXS peak that is centered at ~0.03 $Å^{-1}$. The crystalline reflections are positively correlated, while the amorphous halo is negatively correlated with the SAXS peak. Hence, this heterospectral pattern is characteristic of rapid propagation of primary lamellae in an unconstrained melt, with polymer crystals organizing into lamellae with an average long period of ~21 nm.

The secondary-irreversible crystallization regime is characterized by a shift in the SAXS peak at nearly constant intensity (Figure 3) as well as a growth of both the WAXS crystalline reflections and the portion of the amorphous halo immediately adjacent to the (110) reflection (1.4−1.46 $Å^{-1}$ in Figure 4). The heterospectral pattern characteristic of secondary-irreversible crystallization exhibits a change in sign of the correlation intensity along the SAXS q-axis. The shift in the SAXS peak position causes the WAXS crystalline reflections to be correlated both positively (for q > 0.03 $Å^{-1}$, where SAXS intensity increases) and negatively (for q < 0.03 $Å^{-1}$, where SAXS intensity decreases) with the SAXS intensity (Figure 10). The negative peaks centered at (0.022 $Å^{-1}$, 1.51 $Å^{-1}$) and (0.022 $Å^{-1}$, 1.65 $Å^{-1}$) indicate the simultaneous increase in intensity of the crystalline reflections and the decrease of intensity in the low-q side of the SAXS peak. These features indicate that crystallites form in the noncrystalline layers of the lamellar stacks having the largest long periods. Positive features centered at (0.048 $Å^{-1}$, 1.51 $Å^{-1}$) and (0.048 $Å^{-1}$, 1.66 $Å^{-1}$) show that these new crystallites increase scattering due to structures having a smaller long period. Hence, the development of crystallinity in the secondary-irreversible crystallization regime is attributed to secondary lamellae that form between already-formed lamellae. Furthermore, the secondary lamellae preferentially form in the thickest noncrystalline layers (i.e., in lamellar stacks with the largest long period), essentially cutting the original long period in half from 28 to 13 nm.

In the reversible regime, heterospectral analysis reveals relationships that were not immediately apparent from the 1D data

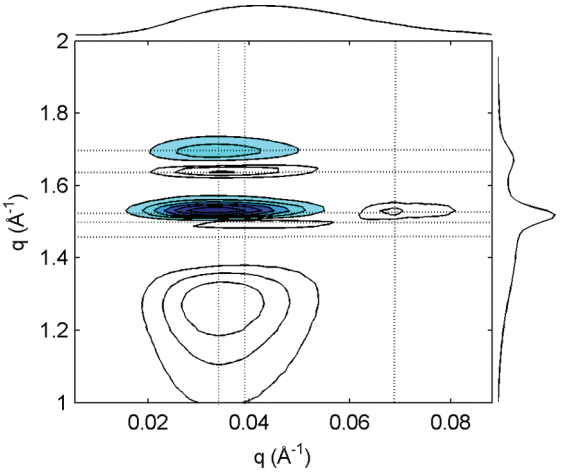

Figure 11. 2D heterospectral correlation plots computed from Lorentz-corrected SAXS and WAXS (horizontal and vertical axes, respectively) obtained during cooling at 10 °C/min in the reversible crystallization regime of L152. Positive and negative contours are shown as open and filled, respectively. Averaged 1D scattering profiles are shown on the sides. The dotted lines on the SAXS axis are at 0.034, 0.039, and 0.070 $Å^{-1}$, and those on the WAXS axis are at 1.46, 1.50, 1.53, 1.64, and 1.70 $Å^{-1}$ (see text).

or from the conventional 2D correlation analysis of SAXS and WAXS individually. Specifically, the heterospectral plot exhibits two positive features centered at (0.068 $Å^{-1}$, 1.53 $Å^{-1}$) and (0.068 $Å^{-1}$, 1.70 $Å^{-1}$) that unambiguously correlate increases at the two crystalline reflections with the formation of entities with a characteristic size of ~9.0 nm manifested in SAXS scattering at large q (Figure 11).

This heterospectral pattern, characteristic of fringed micelle formation in fully constrained melt, exhibits changes in sign of the correlation intensity along both the SAXS and WAXS q-axis (horizontal and vertical direction in Figure 11, respectively).

Table 2. Summary of Crystallization Behavior of HPBD Materials

	crystallization regimes		
	primary-irreversible	secondary-irreversible	reversible
morphological parameters	X_c, L_p, and Q vary strongly with T; hysteresis between cooling and heating	Q is near maximum, while X_c and L_p change with T, showing hysteresis (cooling/heating)	X_c, L_p, and Q change with T, but *no* hysteresis between cooling and heating
SAXS	peak intensity grows as T is reduced	constant peak intensity	peak intensity decreases
	peak position moves to higher q in all 3 crystallization regimes		
WAXS	decrease in intensity of amorphous halo as T is reduced	change in shape and position of amorphous halo	strong change in shape and position of amorphous halo
	crystalline peaks grow in intensity, broaden, and move to higher q in all 3 crystallization regimes		
2D hetero SAXS/WAXS physical interpretation	intensity redistribution in WAXS primary lamellar growth in unconstrained melt	intensity redistribution in SAXS secondary lamellar growth in constrained melt within the largest noncrystalline regions between primary lamellae	intensity redistribution in SAXS and WAXS fringed micelle formation in severely constrained melt within remaining noncrystalline layers

Negative peaks at (0.034 Å^{-1}, 1.53 Å^{-1}) and (0.034 Å^{-1}, 1.70 Å^{-1}) indicate the formation of crystallites (increase in WAXS at 1.53 and 1.70 Å^{-1}, corresponding to unit cell parameters a = 7.39 Å and b = 4.94 Å typical of PE crystals near room temperature[52,53]) coincides with a decrease in SAXS scattering at 0.033 Å^{-1}, corresponding to a long period of 19 nm (Figure 11). Thus, reversible crystallites preferentially form in noncrystalline layers that were too small to permit growth of secondary lamellae. Positive features centered at (0.039 Å^{-1}, 1.50 Å^{-1}) and (0.034 Å^{-1}, 1.64 Å^{-1}) indicate a decrease in WAXS scattering from crystals with unit cell dimensions of a = 7.66 Å and b = 5.00 Å as they contract during cooling from 63 to 0 °C. These dimensions are greater than expected below 60 °C,[43,44] suggesting that the decrease in WAXS occurs preferentially in the high-end of the unit cell size distribution.

No correlation was observed between SAXS intensity changes and the WAXS feature at 1.46 Å^{-1} in the synchronous plot (Figure 7, lower left). Therefore, changes in WAXS during reversible crystallization occur without evidence of a mesophase in SAXS. Changes in WAXS are again accounted for by variations in position and shape of only the amorphous halo and the crystalline reflections; there is no apparent need to invoke a semiordered phase.

Although not discussed here, further insights may also be gained from supplemental tools such as normalization.[17]

CONCLUSION

Two-dimensional correlation analysis, which is well-established in the field of vibrational spectroscopy,[7,15,16,36] proved useful in analyzing X-ray scattering data and elucidating physical phenomena associated with quiescent crystallization of an ethylene copolymer. Morphology evolution in the three crystallization regimes of random copolymers—primary-irreversible, secondary-irreversible, and reversible—resulted in unique signatures in conventional 2D correlation plots of WAXS and SAXS as well as 2D heterospectral correlation patterns (Table 2).

Heterospectral analysis provided insight about the direct relationship between a growing population of crystalline unit cells (WAXS) and their organization into superstructures (SAXS). Propagation of primary lamellae through unconstrained melt during primary-irreversible crystallization is characterized by SAXS−WAXS correlation features that are negative at low WAXS wavevectors (consumption of noncrystalline material) and positive at high WAXS wavevectors (growth of crystalline diffraction peaks; Figures 9−11). During secondary-irreversible crystallization, growth of secondary lamellae in the largest noncrystalline layers between primary lamellae gives SAXS−WAXS heterocorrelation features that are negative and positive at low and high SAXS wavevectors, respectively (Figure 10). Fringed-micelle formation in severely constrained noncrystalline regions is characterized by changes in the sign of the correlation intensity along both the SAXS and WAXS wavevectors (Figure 11). These heterospectral patterns can be used to fingerprint the corresponding physical processes in other polymer systems.

No evidence was found for the formation of a semiordered phase that has been proposed in previous studies.[4,5,21,22,24] Those WAXS features that might be attributed to a semiordered phase do not vary together as they would if they arose from the same underlying phase. Instead, these features are ascribed to thermal contraction of the crystalline phase, loss of coherent unit cell growth at low temperatures, and a change in shape and position of the amorphous halo. The latter observation is explained by thermal contraction of the noncrystalline material and its enrichment with ethyl groups near the crystal surface. The rejection of short-chain branches increases crowding at the crystal interface, resulting in heterogeneity in the noncrystalline phase. This heterogeneity is evident when crystallites form in a constrained melt (i.e., secondary lamellae and fringed micelles).

Further examination of materials with varying SCB content using 2D correlation analysis may give further insight into the development of this heterogeneity. One would expect that the amount of noncrystalline heterogeneity would increase with crystal defects.[24,45] Two-dimensional correlation analysis of WAXS data proved to be highly sensitive to changes, revealing, for example, subtle, yet important features of fringed micelle formation. This sensitivity of 2D correlation analysis makes it a powerful tool to study materials with different crystal morphs that are difficult to resolve from 1D curves, such as "double crystalline" block copolymers.[54]

AUTHOR INFORMATION

Corresponding Author
*E-mail: jak@cheme.caltech.edu.

ACKNOWLEDGMENT

We thank ExxonMobil Research and Engineering Company (Clinton, NJ) and funding from the National Science Foundation (DMR-0505393 and GOALI-0523083). We thank the beamline scientists at X27C at NSLS BNL (Dr. Lixia Rong and Jie Zhu). Important preliminary experiments were performed at 7.3.3 at ALS LBL with assistance from Dr. Alexander Hexemer and Eliot Gann, as well as Zuleikha Kurji (Caltech). We thank Maria Xenidou and Charles Symon for the synthesis of the polymer used in this study.

REFERENCES

(1) Goderis, B.; Peeters, M.; Mathot, V. B. F.; Koch, M. H. J.; Bras, W.; Ryan, A. J.; Reynaers, H. *J. Polym. Sci., Part B: Polym. Phys.* **2000**, *38*, 1975–1991.
(2) Mathot, V. B. F.; Scherrenberg, R. L.; Pijpers, M. F. J.; Bras, W. *J. Therm. Anal.* **1996**, *46*, 681–718.
(3) McFaddin, D. C.; Russell, K. E.; Wu, G.; Heyding, R. D. *J. Polym. Sci., Part B: Polym. Phys.* **1993**, *31*, 175–183.
(4) Sajkiewicz, P.; Hashimoto, T.; Saijo, K.; Gradys, A. *Polymer* **2005**, *46*, 513–521.
(5) Russell, K. E.; Hunter, B. K.; Heyding, R. D. *Eur. Polym. J.* **1993**, *29*, 211–217.
(6) Fernandez-Ballester, L.; Gough, T.; Meneau, F.; Bras, W.; Ania, F.; Balta-Calleja, F. J.; Kornfield, J. A. *J. Synchrotron Radiat.* **2008**, *15*, 185–190.
(7) Noda, I. In *Recent Advancement in the Field of Two-Dimensional Correlation Spectroscopy*; 2008; Elsevier Science BV: Amsterdam, 2008; pp 2−26.
(8) Noda, I. Dynamic Infrared Dichroism and Two-Dimensional Correlation Spectroscopy. Univeristy of Tokyo, 1997.
(9) Kim, H. J.; Bin Kim, S.; Kim, J. K.; Jung, Y. M. *J. Phys. Chem. B* **2006**, *110*, 23123–23129.
(10) Alizadeh, A.; Richardson, L.; Xu, J.; McCartney, S.; Marand, H.; Cheung, Y. W.; Chum, S. *Macromolecules* **1999**, *32*, 6221–6235.
(11) Rabiej, S.; Goderis, B.; Janicki, J.; Mathot, V. B. F.; Koch, M. H. J.; Groeninckx, G.; Reynaers, H.; Gelan, J.; Wlochowicz, A. *Polymer* **2004**, *45*, 8761–8778.
(12) Androsch, R.; Wunderlich, B. *J. Polym. Sci., Part B: Polym. Phys.* **2003**, *41*, 2157–2173.
(13) Nam, J. Y.; Kadomatsu, S.; Saito, H.; Inoue, T. *Polymer* **2002**, *43*, 2101–2107.
(14) Goderis, B.; Reynaers, H.; Koch, M. J. *Macromolecules* **2002**, *25*, 5840–5853.
(15) Noda, I. *Appl. Spectrosc.* **2000**, *54*, 994–999.
(16) Noda, I.; Ozaki, Y. *Two-Dimensional Correlation Spectroscopy*; John Wiley & Sons Ltd.: West Sussex, 2004.
(17) Smirnova, D. S. Application of Two-Dimensional Correlation Analysis to Explosives Detection and Polymer Crystallization. California Institute of Technology, Pasadena, CA, 2009.
(18) Noda, I. *Appl. Spectrosc.* **1990**, *44*, 550–561.
(19) Jia, Q.; Wang, N. N.; Yu, Z. W. *Appl. Spectrosc.* **2009**, *63*, 344–353.
(20) Simanke, A. G.; Alamo, R. G.; Galland, G. B.; Mauler, R. S. *Macromolecules* **2001**, *34*, 6959–6971.
(21) Baker, A. M. E.; Windle, A. H. *Polymer* **2001**, *42*, 667–680.
(22) Rabiej, S.; Bnias, W.; Binias, D. *Fibres Text. East. Eur.* **2008**, *16*, 57–62.
(23) Rabiej, S. In *WAXS Investigations of the Amorphous Phase Structure in Linear Polyethylene and Ethylene-1-Octene Homogeneous Copolymers*; Inst Chemical Fibres: 2005; pp 30−34.
(24) Monar, K.; Habenschuss, A. In *Modeling the Principal Amorphous Halo in Quiescent Melts of Polyethylene and Ethylene Copolymers Using Wide-Angle X-ray Scattering and Its Implications*; John Wiley & Sons Inc.: New York, 1999; pp 3401−3410.
(25) Androsch, R.; Blackwell, J.; Chvalun, S. N.; Wunderlich, B. *Macromolecules* **1999**, *32*, 3735–3740.
(26) Kolesov, I. S.; Androsch, R.; Radusch, H. J. In *Non-isothermal Crystallization of Polyethylenes As Function of Cooling Rate and Concentration of Short Chain Branches*; Kluwer Academic Publ.: Norwell, MA, 2004; pp 885−895.
(27) Androsch, R.; Wunderlich, B. *Macromolecules* **2000**, *33*, 9076–9089.
(28) Hu, W. G.; Srinivas, S.; Sirota, E. B. *Macromolecules* **2002**, *35*, 5013–5024.
(29) Azzurri, F.; Gomez, M. A.; Alfonso, G. C.; Ellis, G.; Marco, C. In *Time-Resolved SAXS/WAXS Studies of the Polymorphic Transformation of 1-Butene/Ethylene Copolymers*; Marcel Dekker Inc.: New York, 2004; pp 177−189.
(30) Hadjichristidis, N.; Xenidou, M.; Iatrou, H.; Pitsikalis, M.; Poulos, Y.; Avgeropoulos, A.; Sioula, S.; Paraskeva, S.; Velis, G.; Lohse, D. J.; Schulz, D. N.; Fetters, L. J.; Wright, P. J.; Mendelson, R. A.; Garcia-Franco, C. A.; Sun, T.; Ruff, C. J. *Macromolecules* **2000**, *33*, 2424–2436.
(31) Rachapudy, H.; Smith, G. G.; Raju, V. R.; Graessley, W. W. *J. Polym. Sci., Part B: Polym. Phys.* **1979**, *17*, 1211–1222.
(32) Driva, P.; Iatrou, H.; Lohse, D. J.; Hadjichristidis, N. *J. Polym. Sci., Part A: Polym. Chem.* **2005**, *43*, 4070–4078.
(33) Koutalas, G.; Iatrou, H.; Lohse, D. J.; Hadjichristidis, N. *Macromolecules* **2005**, *38*, 4996–5001.
(34) The author would like to thank Lixia Rong and Jie Zhu with beamline assistance.
(35) Cser, F. *J. Appl. Polym. Sci.* **2001**, *80*, 2300–2308.
(36) Noda, I. *Appl. Spectrosc.* **1993**, *47*, 1329–1336.
(37) Flory, P. J. *Trans. Faraday Soc.* **1955**, *51*, 848–857.
(38) Alfrey, T.; Goldfinger, G. *J. Chem. Phys.* **1944**, *12*, 205–209.
(39) Mayo, F. J.; Lewis, F. K. *J. Am. Chem. Soc.* **1944**, *66*, 1594–1601.
(40) Tosi, C. *Adv. Polym. Sci.* **1968**, *5*, 451–462.
(41) Czarnecki, M. A. *Appl. Spectrosc.* **1998**, *52*, 1583–1590.
(42) Morita, S.; Miura, Y. F.; Sugi, M.; Ozaki, Y. *Chem. Phys. Lett.* **2005**, *402*, 251–257.
(43) Watanabe, S.; Sano, N.; Noda, I.; Ozaki, Y. *J. Phys. Chem. B* **2009**, *113*, 3385–3394.
(44) Knudsen, K. D.; Hemmingsen, P. V.; We, F. *Polymer* **2007**, *48*, 3148–3161.
(45) Alamo, R.; Domszy, R.; Mandelkern, L. *J. Phys. Chem.* **1984**, *88*, 6587–6595.
(46) Shirayama, K.; Watabe, H.; Kita, S. *Makromol. Chem.* **1972**, *151*, 97–&.
(47) Swan, P. R. *J. Polym. Sci.* **1962**, *56*, 409–.
(48) Perez, E.; Benavente, R.; Quijada, R.; Narvaez, A.; Galland, G. B. *J. Polym. Sci., Part B: Polym. Phys.* **2000**, *38*, 1440–1448.
(49) Peeters, M.; Goderis, B.; Vonk, C.; Reynaers, H.; Mathot, V. *J. Polym. Sci., Part B: Polym. Phys.* **1997**, *35*, 2689–2713.
(50) Howard, P. R.; Crist, B. *J. Polym. Sci., Part B: Polym. Phys.* **1989**, *27*, 2269–2282.
(51) Qiu, J.; Xu, D.; Zhao, J.; Niu, Y.; Wang, Z. *J. Polym. Sci., Part B: Polym. Phys.* **2008**, *46*, 2100–2115.
(52) Swan, P. R. *J. Polym. Sci.* **1962**, *56*, 403–.
(53) In *Wiley Database of Polymer Properties*; John Wiley & Sons, Inc.: New York, 1999−2009.
(54) Hamley, I. W.; Parras, P.; Castelletto, V.; Castillo, R. V.; Muller, A. J.; Pollet, E.; Dubois, P.; Martin, C. M. *Macromol. Chem. Phys.* **2006**, *207*, 941–953.